Journal of Materials Chemistry A

Accepted Manuscript

ROYAL SOCIETY OF CHEMISTRY

www.rsc.org/materialsA

Table of contents entry

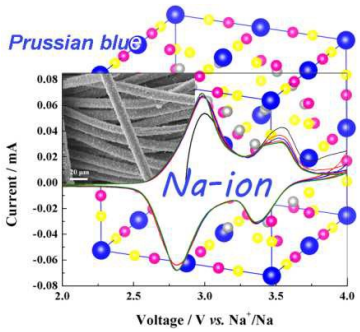

Flexible metal-organic frameworks composed of Prussian blue analogues on a highly conductive carbonfiber paper have been synthesized and utilized as attractive host for sodium ion storage at ambient temperature.

Journal Name

ARTICLE

Flexible Metal-organic Frameworks as Superior Cathodes for Rechargeable Sodium-ion Batteries

Received 00th January 20xx,
Accepted 00th January 20xx

DOI: 10.1039/x0xx00000x

www.rsc.org/

Ping Nie, Laifa Shen, Gang Pang, Yaoyao Zhu, Guiyin Xu, Yunhua Qing, Hui Dou, and Xiaogang Zhang*

In response to the ever-increasing demand for grid-scale energy storage systems, sodium ion batteries (SIBs) working at ambient-or room-temperature are gaining much attention as promising alternatives because of the abundance and low cost of sodium resources. However, their adoption is significantly hampered by several issues, especially in terms of sluggish kinetics and capacity retention during cycling. Herein, flexible Prussian blue analogue $FeFe(CN)_6$/carbon cloth composites are synthesized using low temperature strategies and utilized as a potential host for sodium ion insertion. As a proof of concept, the composites demonstrate excellent electrochemical performance: reversible specific capacity of 82 mAh g^{-1} at 0.2C, good rate capability and long term cycling life with 81.2% capacity retention over 1000 cycles. Most significantly, this low-cost, scalable and low-temperature synthesis provides guidance for the design of other flexible materials that could have applications in wearable electronics, energy storage and conversion devices.

Introduction

Advanced energy storage technologies are urgently needed to meet the continuously surging demand for emerging applications including electric vehicles and grid-level energy storage for intermittent power sources produced from wind and solar energy.[1-3] Lithium-ion batteries (LIBs) have enjoyed great success for portable electronics in the past two decades, and currently being intensively pursued for transportation due to their reasonable durability, small spatial footprint, superior power and energy densities.[4, 5] Nevertheless, the main barrier is the high cost and partly safety considerations. Currently, LIBs manufactured for consumer electronics cost several hundred dollars per stored energy (kWh). But for vehicle applications, the cost must come down closer to USD100/kWh, and it should be cheaper still for grid applications. The expensive lithium resources and accessible global lithium reserves greatly lead to the controversies for the mass production of energy storage devices. The exploration for alternative new battery concepts beyond LIBs using naturally abundant materials have thus attracted increasing attention.[6, 7]

Ambient temperature sodium-ion batteries are one of the promising candidates in this regard due to the worldwide abundance and low cost of sodium resources, also better safety compared to high-temperature Na/S and $Na/NiCl_2$ Zebra cells.[8-11] Similar to Li-ion batteries, the SIBs operate following a "rock chair" concept, in which Na^+ deintercalates from one electrode, diffusing through the electrolyte, and then inserts into the other electrode materials. Additionally, electrolytes with lower decomposition potential can be used and electrolyte degradation will be reduced in Na-ion batteries owing to the lower standard potential of sodium (E^0 = -2.71 V *vs.* SHE) compared with lithium (-3.04 V *vs.* SHE). In particular, the ability to use aluminum current collector for anode must be effective for further battery manufacture cost reduction.[12] Despite these distinct advantages, the practical application of Na-ion battery is hindered by several issues, including a much larger radius of Na^+ (1.02 Å, ~55% larger than Li^+ of 0.76 Å), three times heavier than lithium (23 g mol^{-1} compared with 6.9 g mol^{-1}), which leads to sluggish kinetics of Na^+ transport and insertion/deinsertion in electrochemical process. Therefore, considerable improvements have been continuously made to design and prepare novel electrodes with enhanced electrochemical performances for advanced Na-ion technologies.

To date, various potential sodium intercalation cathode materials and new electrolytes have been extensively investigated for applications in SIBs.[13-15] Layered Na transition metal oxides, such as P2-$Na_x[Fe_{1/2}Mn_{1/2}]O_2$ is potential candidate for high capacity positive electrodes, which could delivers a reversible capacity of 190 mAh g^{-1} with the Fe^{3+}/Fe^{4+} redox couples.[16] The energy density of P2-type $Na_{2/3}[Ni_{1/3}Mn_{2/3}]O_2$ achieves 540 Wh kg^{-1} in half-cell based on sodium metal anode, but both of them suffer from insufficient cyclability and poor kinetics.[17] Triphylite-type $NaFePO_4$ shows

College of Material Science and Engineering, Jiangsu Key Laboratory of Materials and Technologies for Energy Conversion
Nanjing University of Aeronautics and Astronautics
Nanjing 210016, Jiangsu, China
E-mail: azhangxg@nuaa.edu.cn

† Electronic Supplementary Information (ESI) available: [Supplementary characterization including FESEM and TEM images, XRD pattern, Infrared spectrum, charge-discharge voltage curves, CV curves, cycling performance, *ex-situ* Mössbauer spectra]. See DOI: 10.1039/x0xx00000x

great thermal stability (up to 480℃) and promising theoretical capacity of 154 mAh g^{-1}.[18] Nevertheless, larger unit cell volume expansion was observed, and the materials are usually obtained by ion-exchange reaction of $LiFePO_4$. NASICON-type $Na_3V_2(PO_4)_3$ and its fluorophosphates exhibit superior rate capability and excellent cycling performance.[19, 20] Around 50% of the initial capacity was obtained over 30,000 cycles at 40C (4.7 A g^{-1}) reported by Balaya's group[21] as well as the ultrafast Na-storage in carbon-coated nanosized $Na_3V_2(PO_4)_3$ embedded in a porous carbon matrix, delivering a specific capacity of 44 mAh g^{-1} a current density up to 200 C.[22] Compared with that obtained in Li-ion electrode, the reversible specific capacity of bulk sodium ion intercalation is usually limited to approximately 120 mAh g^{-1}. Thus, it is of both academic and practical significance in the SIBs field to discover and tailor new cathode materials to achieve high Na-storage capacity and long term stability.

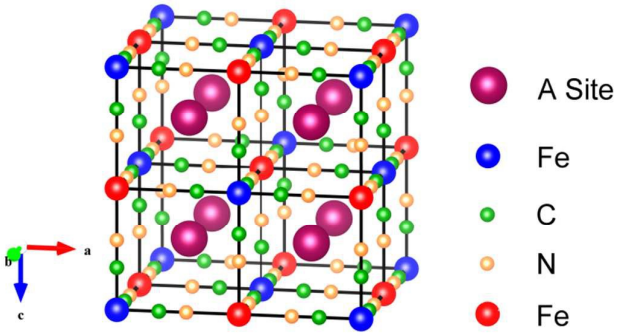

Scheme 1. Schematic diagram of the unit cell of the open-framework $FeFe(CN)_6$ Prussian blue analogue structure.

Owing to their unique structural features, coordination polymers (CPs), including metal-organic frameworks (MOFs, an emerging class of materials made from metal ion and organic ligands),[23] and porous coordination polymers (PCPs)[24] have aroused intense research interest because of their numerous promising applications in the field of gas storage,[25] catalysis,[26] magnetism,[27, 28] luminescence,[29] and sensing applications.[30, 31] Recently, their unique combination of optical and electronic properties has led to interest in incorporating them into photovoltaic and electrochemical devices.[32, 33] Vittal *et al.*[34, 35] firstly investigated the electrochemical performance of metal organic-phosphate open frameworks as a new class of cathode materials for lithium ion batteries, and the utilization of oxalatophosphate framework as a single source precursor for the synthesis of inorganic material.[36] Among the reported MOFs, Prussian blue and its analogues (PBAs) have recently been explored for various applications ranging from separation, catalysis, molecular magnetics and energy storage. Our group recently reported promising utilization of PBAs as new precursors for nanoporous inorganic materials preparation In LIBs.[37] A bi-functional device for self-powered electrochromic window and transparent battery by using Prussian blue as an electrode has been demonstrated by Lou and co-workers.[38] Wessells *et al.*[39, 40]demonstrated reversible insertion/extraction of sodium and potassium ions in nickel/copper hexacyanoferrate nanoparticles with superior rate capabilities and extremely long cycling stability when operated in inexpensive aqueous electrolytes. Full open-framework aqueous batteries were reported by combining the copper hexacyanoferrate cathode with activated carbon/polypyrrole composite anode,[41] also a newly developed manganese hexacyanomanganate open-framework anode.[42] All the battery systems exhibited high efficiency and excellent capacity retention for ultralong cycle, which make PBAs desirable for stationary energy storage application. Moreover, the electrochemical Na^+/Li^+ intercalation into PBAs have been investigated in organic electrolytes.[43, 44] Very recently, Prussian blue analogues are also demonstrated as potential host for various di-/tri-valent charge carrier ions, such as Mg^{2+}, Ca^{2+}, Sr^{2+}, Ba^{2+} and Al^{3+} in aqueous electrolytes.[45-48] Prussian blue analogues have a general formula of $A_xP[R(CN)_6]_y\cdot\square_{1-y}\cdot nH_2O$, A: alkali cations; P, R: transition metal; and □: $[R(CN)_6]$ vacancy, where transition metal ions are bridged to the cyanide ligands forming a cubic face-centered structure (Scheme 1). Large interstitial 'A sites' within the structure can host zeolitic water, hydrated alkali and di-/tri-valent ions.[49] In the open-framework, guest cations can occupy large interstitial 'A sites' around the center of each cube sub-cell, and the large channels oriented in the <100> directions allow rapid transport of these ions throughout the lattice, thus enabling the insertion and rapid diffusion of a wide variety of ions, and small molecule with very little lattice strain.[45, 50]

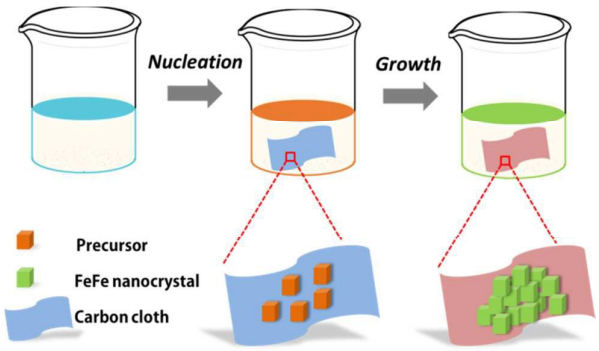

Figure 1. Schematic illustration of the process used for the synthesis of $FeFe(CN)_6$/carbon cloth composites.

The concerns about the Prussian blue analogues are their insufficient cycle life and low energy efficiency in non-aqueous electrolytes for sodium-ion batteries, associated with the low electrical conductivity and structural imperfection.[51, 52] In this work, we report a significant advance in the design and preparation of Prussian blue analogues $FeFe(CN)_6\cdot xH_2O$[53] nanoparticles on a flexible carbonfiber paper as a binder-free cathode in both organic and aqueous electrolytes. This electrode structure design with high conductive scaffold for loading electroactive materials effectively prevents loss of active mass and enhances electrical contact, which make it an ideal candidate for use in SIBs. The configuration can also significantly simplify the battery packing process. To the best of our knowledge, the environmentally friendly and good

economy candidate grown on flexible conductive substrates has not been studied yet. The Na-ion insertion/extraction mechanism and significantly improved sodium storage were examined by *ex situ* ^{57}Fe Mössbauer spectroscopy. With the merits of carbon cloth paper such as flexible structure and high conductivity, the resulting $FeFe(CN)_6 \cdot xH_2O$ nanocomposite electrode exhibits reversible specific capacity of 82 mAh g^{-1} at 0.2C, prolonged cycling performance with 81.2% capacity retention for 1000 cycles, and good high rate response up to 10C.

Results and discussion

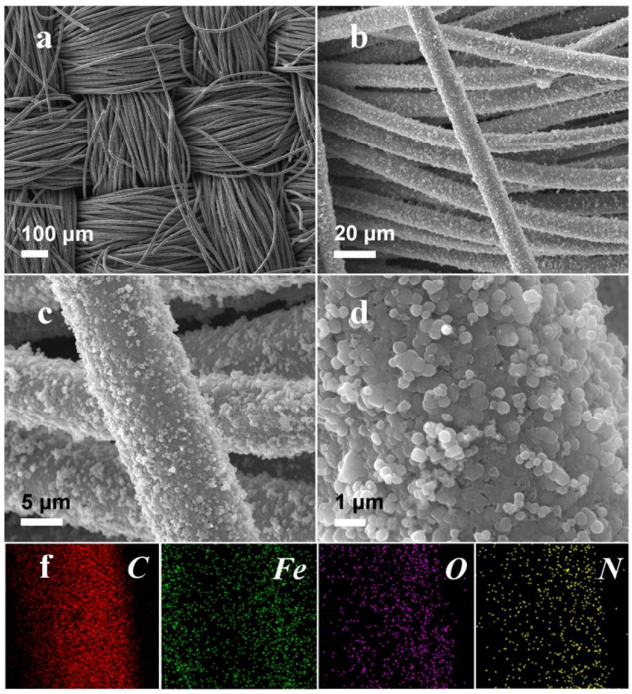

Figure 2. a, b) Low and c, b) high magnification SEM images of the $FeFe(CN)_6$/carbon textiles, f) the EDS mapping for the composites.

Carbonfiber paper with high flexibility and conductivity was used as the growth substrates for the $FeFe(CN)_6$ Prussian blue analogues. The fabrication of the $FeFe(CN)_6$/carbonfiber composites were realized simply by a solution precipitation route at elevated temperature of 60 ℃ (see Figure 1). Firstly, concentrated nitric acid was chosen to activate the surface of carbonfiber paper to increase the binding sites and adhesion between carbonfiber paper and $FeFe(CN)_6$ nanoparticles.[54] Subsequently, $FeFe(CN)_6$ nanoparticles were directly grown on the conductive carbonfiber paper substrates by a facile solution precipitation method. After the synthesis, the color of the carbonfiber paper changed from black to dark green, suggesting that $FeFe(CN)_6$ nanoparticles have grown successfully. Importantly, the resulting film exhibits good flexibility and mechanical properties under bending with a tweezer, which can be directly used as a free-standing electrode for sodium ion batteries (Figure S1).

The morphology of the products was examined with field-emission scanning electron microscope (FESEM). The low SEM image (Figure 2a) of $FeFe(CN)_6$/carbon cloth composites dispalys an overview of the three-dimensional texture structure, where the woven carbon cloth consisting of many carbon fibers serves as an excellent conductive scaffold for uniform growth of the $FeFe(CN)_6$ nanoparticles. The carbon fibers keep the ordered woven structure of the carbon cloth after the crystal growth of $FeFe(CN)_6$, but exhibit a rougher surface as compared to that of the pure carbon cloth (Figure 2b, c, Figure S2), indicating that the carbon cloth has been covered with $FeFe(CN)_6$ product. The magnified FESEM images in Figure 2d reveal that the $FeFe(CN)_6$ nanoparticles uniformly cover carbonfiber paper and they interconnect with each other to form an integrated structure. Figure 2f displays corresponding energy dispersive X-ray spectroscopy (EDS) of $FeFe(CN)_6$/carbon cloth composites, which confirm that the formation of pure $FeFe(CN)_6$ and uniform distribution of iron, carbon, nitrogen and oxygen components throughout the composite. To gain further information on the microstructure of the composites, Transmission electron microscopy (TEM) measurement was carried out. As shown in Figure S3, the size of $FeFe(CN)_6$ nanoparticles is estimated to be approximately 200 nm, consistent with the SEM results. Furthermore, the selected-area electron diffraction (SAED) pattern (Figure S3b) clearly demonstrated the single crystalline nature of the nanoparticles. In comparison, only agglomerations of $FeFe(CN)_6$ nanoparticles with the size of 200~400 nm will be formed under similar synthesis conditions in the absence of carbon cloth substrates (Figure S4).

The crystallographic structure of the samples was further analyzed by powder X-ray diffraction (XRD). Figure 3a shows the XRD patterns of the as-prepared $FeFe(CN)_6$/carbon textiles and bare $FeFe(CN)_6$ nanoparticles. All the diffraction peaks can be readily indexed to a face-centered cubic structure (space group Fm-3m), in good accordance with the results reported in the literature.[51, 55] Additional reflections at around 26.2° and 43.1° highlighted by asterisk in the $FeFe(CN)_6$/carbon textile composite originate from the carbon cloth (Figure S5).[56, 57] Toward smaller crystallite size, reflections from $FeFe(CN)_6$/carbon textiles are significantly broad and their intensity decreases.[58] $Fe^{III}[Fe^{III}(CN)_6] \cdot yH_2O$ is a typical Prussian blue analogue. The structure of ferriferricyanide contains a three-dimensional network of Fe_1-N≡C-Fe_2 chains along the edges of the unit cell cube, where octahedral $Fe^{III}(CN)_6^{3-}$ complexes are bridged into a simple cubic lattice by Fe^{3+} ions, forming a face-centred cubic phase (Scheme 1). The band at 2084.8 cm^{-1} and a broad peak at 3365.8 cm^{-1} were assigned to the stretching vibrations from CN^- and the ν(O-H) of water molecules, respectively, as evidenced by FTIR spectrum (Figure 3b). The composition of $FeFe(CN)_6$ was further confirmed by thermogravimetric analysis (TGA). The initial 15.8 % weight loss below 180 ℃ can be attributed to the removal of weakly bonded and coordinated water molecules in the PBAs, corresponding the loss of 2 water molecules from the structure, indicating hydrated $FeFe(CN)_6 \cdot 2H_2O$ is obtained under the current conditions (Figure S6). The water content is

well consistent with the results of Prussian blue and its analogues electrodes for rechargeable batteries reported in recent references[51, 59, 60], where the corresponding contents of water of nickel ferricyanide, $FeFe(CN)_6$ nanoparticles and $Na_{1.40}MnFe(CN)_6$ are about 34%, 20%, and 17%, respectively. The second weight loss of 30.5% observed between 175 and 275 ℃ is caused by the decomposition and subsequent oxidation of the metal-organic frameworks.

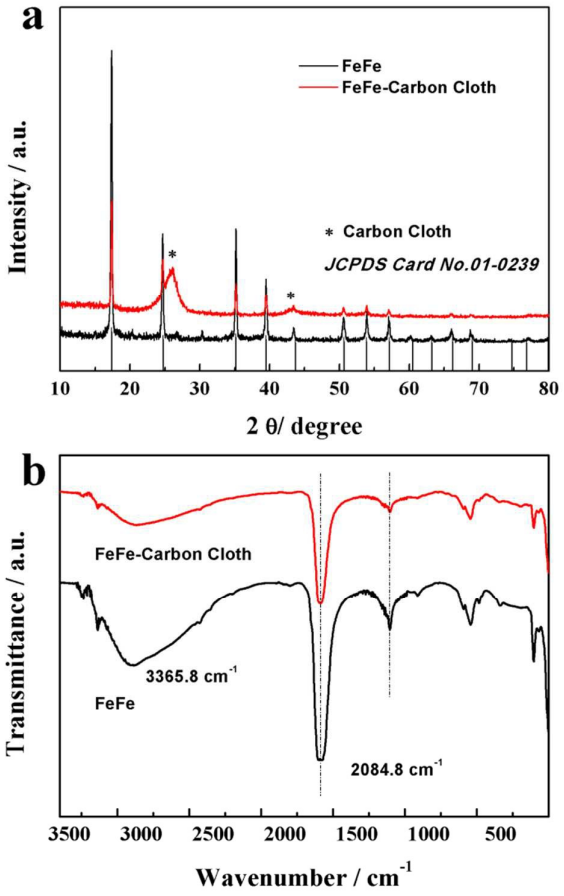

Figure 3. a) XRD patterns of $FeFe(CN)_6$/carbon textiles and bare $FeFe(CN)_6$ nanoparticles, b) Infrared spectrum of the $FeFe(CN)_6$ scratched down from carbon cloth and bare $FeFe(CN)_6$ nanoparticles.

To study the electrochemical properties of the $FeFe(CN)_6$/carbon textile binder free electrode, Coin cells were fabricated with sodium foil as a counter electrode. Figure 4a exhibits the initial five charge/discharge profiles of $FeFe(CN)_6$/carbon textiles at a current density of 0.2C (1C=120 mA g^{-1}), in which two distinguishable charge potential plateau at around 3.1 V and 3.6 V, and discharge potential plateau (2.8 and 3.4 V) appear, consistent with results noted in previous reports and the CV analysis discussed below (Figure 7).[43, 51] The electrode delivered high first-cycle charge and discharge capacities of 83 and 82 mAh g^{-1} respectively, corresponding to an initial Coulombic efficiency of about 98.7 %. From the second cycle, the reversible capacity is stable and maintained at around 81 mAh g^{-1}, implying the outstanding reversibility and stability of the electrodes. Noteworthy, carbon textile

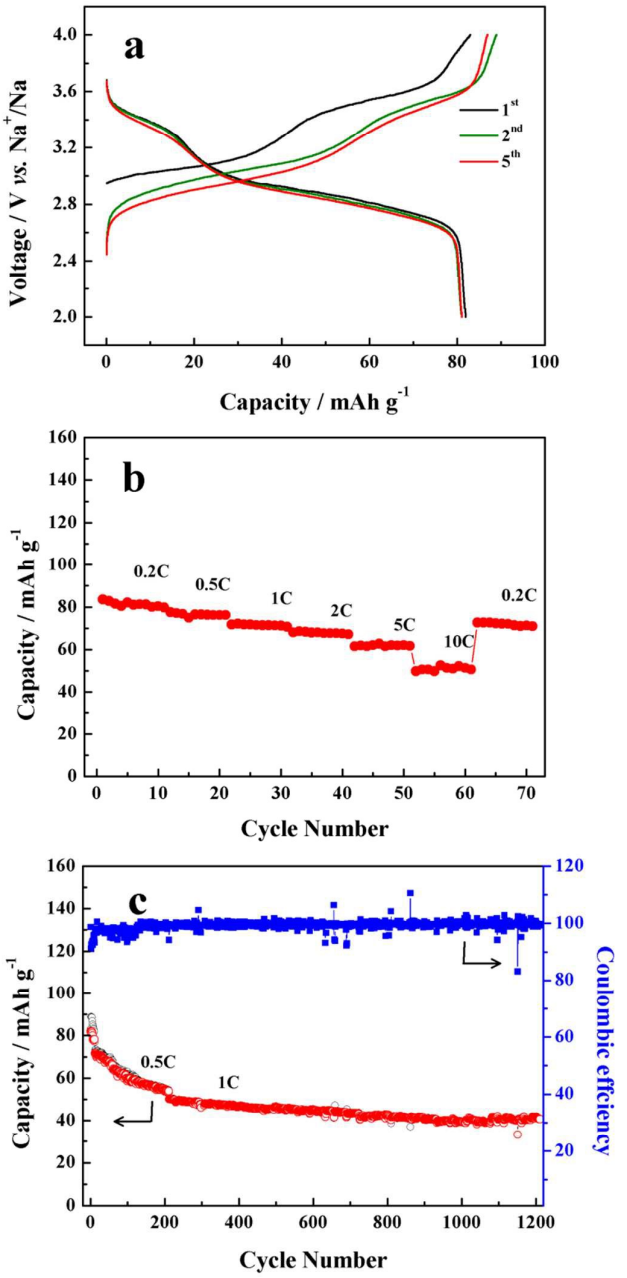

Figure 4. Electrochemical evaluation of $FeFe(CN)_6$/carbon textiles for sodium-ion batteries: a) charge-discharge voltage profiles at a current density of 0.2C, b) rate capability at different current densities between 2.0 and 4.0 V, c) cycling performance at a current density of 0.5 and 1C.

substrate in the composites is electrochemically inactive in the voltage window selected, thus it does not contribute to the observed specific capacity (Figure S7). Figure 4c shows the cycling performance of the $FeFe(CN)_6$/carbon textile at a higher current density of 0.5 and 1C (after initial ten cycles at 0.2C). It clearly reveals that the as-prepared material demonstrated a good cycle life over 1200 charge/discharge cycles. An initial capacity of 72 mA h g^{-1} was achieved at a current rate of 0.5 C. The capacity decreased to 54 mA h g^{-1} after 200 cycles, which represents a capacity fade of 25%.

When the current density was increased to 1.0 C, improved cycle stability was achieved. The cells retained 81.2% of initial capacity at the end of the long-term 1000 cycles at 1C, corresponding to an average capacity decay of 0.019% per cycle. Simultaneously, it also exhibited a high and stable Coulombic efficiency of above 99% after the initial cycles.

Rate capability is another important parameter for evaluating the power applications of sodium ion batteries. To manifest the high-rate performance, the discharge capacities were investigated at different C-rates in the potential range of 2.0 to 4.0 V. As shown in Figure 4b, the composites deliver very high capacities of 83, 77, 72, 69 and 62 mAh g^{-1} at the current densities of 0.2, 0.5, 1, 2 and 5C, respectively. Importantly, the capacity was recovered when the current was reduced to initial 0.2C after 70 cycles, indicating high reversibility of the electrode. The electrochemical impedance spectroscopy measurements were performed on fresh cells with amplitude of 5 mV in frequencies from 100 kHz to 0.01 Hz (Figure S8). Both Nyquist plots comprise two parts including a depressed semicircle in high frequency and a linear Warburg part in a low frequency. Obviously, the $FeFe(CN)_6$/carbon textiles electrodes show smaller diameter of semicircles in the Nyquist plots than those of the corresponding bare $FeFe(CN)_6$ electrodes, thus indicating lower charge-transfer resistance (R_{ct}) and better kinetics for Na^+ insertion/extraction reactions. After 10 cycles at 0.2C, the $FeFe(CN)_6$/carbon cloth electrode has slightly larger impedance (Figure S8), which may be due to the formation of the surface electrolyte interface (SEI) during the cycles, further confirming that the carbon cloth could indeed act as a good substrate for $FeFe(CN)_6$ loading. This improved Na^+ storage properties can be attributed to the high electronic conductivity of carbon textile and the nanoparticles morphology, which facilitate short and fast transport for both electrons and Na^+.

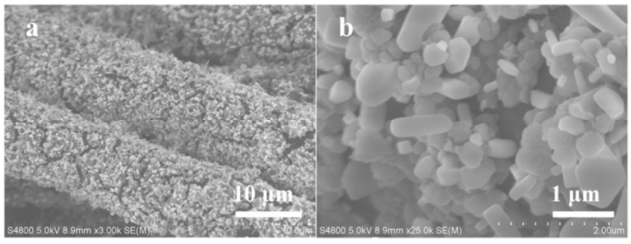

Figure 5. SEM images of $FeFe(CN)_6$/carbon textiles composite after C-rate cycling for 60 cycles at different current densities from 0.2 to 10C (Figure 4b).

The morphology change of $FeFe(CN)_6$/carbon textiles composite after cycling at different current densities from 0.2 to 10C for 60 cycles is shown in Figure 5. Compared with the original samples (Figure 2c, d), the morphology of electrodes becomes rough as the result of the redox reaction. However, it maintains the particles-like morphology, where the $FeFe(CN)_6$ active materials are still connected with the carbon textiles, effectively preventing the pulverization and aggregation of nanoparticles during cycling. X-ray diffraction pattern of the $FeFe(CN)_6$/carbon cloth after 50 cycles further demonstrates the structural stability of the $FeFe(CN)_6$/carbon textiles electrode (Figure S9). The sodium ion and electron can migrate back and forth facilely and rapidly from the active material to the current collector due to the intimate contact between the electroactive material and the conductive carbon fibers cloth, beneficial for high-rate capability and excellent cyclic stability.[61, 62]

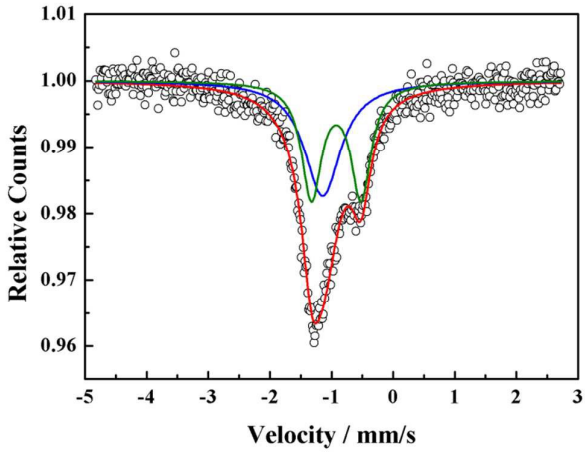

Figure 6. Room-temperature Mössbauer spectrum for pristine $FeFe(CN)_6$ material.

Aqueous rechargeable sodium ion batteries, which offer some compelling merits in terms of safety, low cost, and scalability, have been regarded as promising alternatives for large-scale energy storage applications.[63] Moreover, higher ionic motilities are observed in aqueous electrolytes and thus compensate relatively sluggish kinetics, resulting in high roundtrip efficiency.[64] The electrochemical Na storage of the $FeFe(CN)_6$ electrode was investigated by both cyclic voltammetry and galvanostatic charge-discharge cycles in mildly acidic 1 M $NaNO_3$ (pH=2) aqueous solution owing to the stability of PBAs at acidic pH than in neutral and basic one.[40, 42] As shown in Figure S10a, a pair of very symmetric redox peaks located at 0.01 and 0.18 V were clearly observed in the voltage window of -0.4–0.6 V with respect to saturated calomel electrode (SCE), which can be attributed to the reversible insertion/extraction of sodium ion into PBAs crystal lattice. $FeFe(CN)_6$ was also evaluated by charge-discharge measurements under different current densities ranging from 0.05 A g^{-1} to 2 A g^{-1} (Figure S10b). The $FeFe(CN)_6$ electrode delivers discharge capacities of 53, 24, 10, and 4 mAh g^{-1} at current densities of 0.1, 0.2, 0.5, and 1, A g^{-1}, respectively. However, fast capacity fade was observed with increasing current densities, probably due to the electrode connecting wire corrosion in acidic solution and fast cation migration gradually destroying the crystal structure of $FeFe(CN)_6$ Prussian blue analogue.[65]

Mössbauer spectroscopy was recorded to accurately probe the detailed compositions and local structures of iron in the obtained samples.[66,67] The black dots and red solid lines correspond to the experimental data and fitted results, respectively (Figure 6). Mössbauer spectrum of the pristine $FeFe(CN)_6$ collected at room temperature consists of one singlet sub-spectrum and doublet one, demonstrating the existence of two distinct Fe(III) sites, typical for $FeFe(CN)_6$

Prussian blue analogue.[55, 68] Reaction mechanism was further verified by *ex situ* Mössbauer spectra of $FeFe(CN)_6$ at different states during electrochemical Na^+ intercalation/de intercalation (Figure S11). Figure 7 shows the cyclic voltammograms (CVs) of the $FeFe(CN)_6$/carbon textiles composite electrode in the voltage range of 2.0-4.0 V at a scan rate of 0.1 mV s^{-1}. Two pairs of well-defined redox peaks at 3.53/3.36 V and 2.98/2.80 V, respectively, can be observed, similar to the CV responses of Prussian blue analogue in literature reports.[43, 51, 68-70] Additionally, the CV curves exhibit good reproducibility and similar shapes with increasing cycle number, demonstrating high reversibility and stability during the sodium insertion and extraction. Based on the different coordination sites of the Fe ions as well as previous electrochemistry investigation on Prussian blue analogues, we therefore conclude that the peaks at 2.98/2.80 V correspond to oxidation/reduction of the Fe^{III}/Fe^{II} couple bonding to the N atoms of $C\equiv N^-$ and those at 3.53/3.36 V to the Fe^{III}/Fe^{II} couple coordinated with $C\equiv N^-$ by C atoms, respectively.[43, 51] The

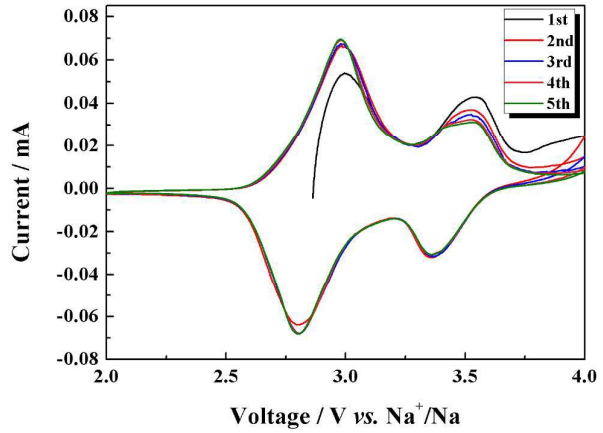

Figure 7. CV curves measured in the voltage of 2.0-4.0 V at a scan rate of 0.1 mV s^{-1}.

redox behaviour occurring in the ferriferricyanide could be described as the electrochemical reaction of Equation 1 and 2:

$Fe^{III}Fe^{III}(CN)_6 + Na^+ + e^- \rightarrow NaFe^{III}Fe^{II}(CN)_6$ (1)

$NaFe^{III}Fe^{II}(CN)_6 + Na^+ + e^- \rightarrow Na_2Fe^{II}Fe^{II}(CN)_6$ (2)

The reason for different electrochemical activity of two Fe atoms in $Fe^{III}Fe^{III}(CN)_6$, especially the voltages and intensities of the reduction and oxidation peaks, has not been fully elucidated despite they exhibit the same oxidization state. Ongoing experiment with *in situ* XRD measurement, Fourier Transform Infrared Spectroscopy and neutron diffraction *etc.* during electrochemical charge-discharge will provide a more complete understanding of the Na^+ insertion reaction in this open framework.[44, 45]

Conclusions

To conclude, we have synthesized flexible $FeFe(CN)_6$/carbon cloth nanocomposites by using a simple solution precipitation method. As a proof of concept, the hybrid demonstrated a specific capacity of 82 mAh g^{-1} at 0.2C rate, good rate capability and cycling performance with 81.2% capacity retention after 1000 cycles. The excellent performance of the $FeFe(CN)_6$/carbon textiles composite benefits from its electrode architectures. Firstly, the $FeFe(CN)_6$ nanoparticles grown directly on the conductive carbon cloth form an integrated electrode, which ensure intimate contacts and fast electron transport between the carbon cloth current collector and the electroactive materials. Secondly, open spaces and loose textures between neighboring carbon fibers endow more efficient penetration of electrolyte into the $FeFe(CN)_6$ nanoparticles and accommodation of the strain induced by the volume change during cycle. Thirdly, the nano-sizes of $FeFe(CN)_6$ active materials provide relatively shorter Na^+ and e^- diffusion paths. Lastly, the binder-free electrodes, avoiding the use of binders or any conducting additives enable a low internal resistance and favorable charge-transfer kinetics. Furthermore, the facial and simple low temperature route used to obtain these environmentally benign positive materials with smaller sizes not only tends to simplify large-scale commercialization but opens new perspectives to develop other flexible Prussian blue and its analogues. These encouraging findings can provides a new insight into the possibility of hierarchical $FeFe(CN)_6$/carbon cloth composites as high-performance flexible sodium ion battery electrodes for large-scale applications in stretchable and bendable energy device in the near future.

Experimental

Materials Synthesis

Commercially available carbon textiles were firstly treated in 65-68 % nitric acid reflux at 80 ℃ for 8 h, then cleaned by deionized water and ethanol for several times, respectively. Typically, 10 mL of 0.1 M $K_3Fe(CN)_6$ solution was added to the same concentration of 20 mL $FeCl_3$ solution during a period of 5 min under agitation at room temperature, followed by the addition of a piece of acid-treated carbon cloth in rectangular shape, and then the resulting solution was maintained at 60 ℃ for 6 h. After cooled down to room temperature naturally, the carbon textiles covered with dark-green product were picked up with tweezers, thoroughly rinsed several times with deionized water and acetone, and dried in air overnight. $FeFe(CN)_6$ nanoparticles were also prepared for comparison in a similar procedure without use of carbon cloth substrate.

Characterization

Field-emission scanning electron microscopy (FESEM, Hitachi S4800) and transmission electron microscopy (HRTEM, JEOL JEM-2100) were employed to observe the morphologies of the samples. The elemental compositions were analyzed by energy dispersive X-ray spectroscopy (EDS) elemental mapping attached to the SEM instrument. Powder X-ray diffraction (XRD) with Cu Kαradiation (Bruker D8 Advance diffractometer) was used to determine the phase composition and crystallinity. Thermogravimetric analysis (TGA) was performed under air flow from 30 to 400 ℃ with a heating rate of 10 ℃ min^{-1}. Fourier transform infrared (FTIR) spectra were obtained on a

Nicolet 750 spectrometer using the KBr pellets in the range of 4000-500 cm^{-1}. The Mössbauer spectra were taken with a Clover Technology Group, Inc. spectrometer with a ^{57}Co γ-ray source, calibrated with α-Fe as standard. The model fitting was performed with WinNormos Igor 6.3 software. The X-ray photoelectron spectroscopy (XPS) was recorded with a Thermo escalab 250Xi spectrometer.

Electrochemical Measurements

The carbon textiles-supported $FeFe(CN)_6$ nanoparticles were directly used as the working electrode without mixing with any binder and conductive additives. The active mass loading was calculated based on the weight difference of the carbonfiber cloth before and after growth. Before weighing, the samples were dried in a vacuum oven at 110 ℃ overnight. Sodium pellets were employed as the counter and reference electrode, a glass microfiber filter and 1 M $NaClO_4$ in ethylene carbonate (EC) and propylene carbonate (PC) (1:1 by vol.) as the separator and electrolytes, respectively. The half-cells were assembled in an argon-filled glove box in the laboratory with low levels of H_2O and O_2 below 1 ppm. For aqueous electrochemical measurement, the electrochemical characterization was carried out using a three-electrode flooded cells, where the electroactive materials grown on the carbon cloth as the working electrodes, Pt foil was served as the counter electrode, a saturated calomel electrode (SCE) as the reference electrode, and 1.0 M $NaNO_3$ aqueous solution at pH=2 purged with N_2 before use as the electrolyte. The galvanostaic charge/discharge and CV measurements were carried out on a Land Battery Test System (Wuhan Kingnuo Electronic Co., China) and CHI660E electrochemical workstation (Chenhua Instruments Co., China). The EIS measurements were carried out on a Solartron 1860/1287 electrochemical interface.

Acknowledgements

The authors are grateful for financial support from the National Program on Key Basic Research Project of China (973 Program, no. 2014CB239701), National Natural Science Foundation of China (no. 21173120, 51372116), Natural Science Foundation of Jiangsu Province (no.BK2011030, BK2011740), Fundamental Research Funds for the Central Universities (NP2014403), a Project Funded by the Priority Academic Program Development of Jiangsu Higher Education Institutions (PAPD), Funding for Outstanding Doctoral Dissertation in NUAA (no.BCXJ14-12), Founding of Graduate Innovation Center in NUAA (no. kfjj201438), Funding of Jiangsu Innovation Program for Graduate Education (no.KYLX_0254) and the China Scholarship Council (no. 201406830023). We also appreciate Dr. Hui Dou and Ms.Yunhua Qing for Mössbauer spectra measurements and analysis.

Notes and references

1. J. M. Tarascon and M. Armand, *Nature*, 2001, **414**, 359-367.
2. B. Dunn, H. Kamath and J.-M. Tarascon, *Science*, 2011, **334**, 928-935.
3. P. Simon, Y. Gogotsi and B. Dunn, *Science*, 2014, **343**, 1210-1211.
4. A. Manthiram, *J. Phys. Chem. Lett.*, 2011, **2**, 176-184.
5. M. V. Reddy, G. V. Subba Rao and B. V. R. Chowdari, *Chem. Rev.*, 2013, **113**, 5364-5457.
6. X. Ji, K. T. Lee and L. F. Nazar, *Nat. Mater.*, 2009, **8**, 500-506.
7. D. Larcher and J. M. Tarascon, *Nat. Chem.*, 2015, **7**, 19-29.
8. J.-J. Braconnier, C. Delmas, C. Fouassier and P. Hagenmuller, *Mater. Res. Bull.*, 1980, **15**, 1797-1804.
9. C. Delmas, J.-J. Braconnier, C. Fouassier and P. Hagenmuller, *Solid State Ionics*, 1981, **3–4**, 165-169.
10. J. M. Paulsen and J. R. Dahn, *Solid State Ionics*, 1999, **126**, 3-24.
11. H. Pan, Y.-S. Hu and L. Chen, *Energy Environ. Sci.*, 2013, **6**, 2338-2360.
12. Y. Kim, K.-H. Ha, S. M. Oh and K. T. Lee, *Chem.–Eur. J.*, 2014, **20**, 11980-11992.
13. V. Raju, J. Rains, C. Gates, W. Luo, X. Wang, W. F. Stickle, G. D. Stucky and X. Ji, *Nano Lett.*, 2014, **14**, 4119-4124.
14. W. Luo, M. Allen, V. Raju and X. Ji, *Adv. Energy Mater.*, 2014, **4**, 1400554.
15. B. Jache and P. Adelhelm, *Angew. Chem. Int. Ed.*, 2014, **53**, 10169-10173.
16. N. Yabuuchi, M. Kajiyama, J. Iwatate, H. Nishikawa, S. Hitomi, R. Okuyama, R. Usui, Y. Yamada and S. Komaba, *Nat. Mater.*, 2012, **11**, 512-517.
17. H. Yoshida, N. Yabuuchi, K. Kubota, I. Ikeuchi, A. Garsuch, M. Schulz-Dobrick and S. Komaba, *Chem. Commun.*, 2014, **50**, 3677-3680.
18. P. Moreau, D. Guyomard, J. Gaubicher and F. Boucher, *Chem. Mater.*, 2010, **22**, 4126-4128.
19. J. Liu, K. Tang, K. Song, P. A. van Aken, Y. Yu and J. Maier, *Nanoscale*, 2014, **6**, 5081-5086.
20. Y. Jiang, Z. Yang, W. Li, L. Zeng, F. Pan, M. Wang, X. Wei, G. Hu, L. Gu and Y. Yu, *Adv. Energy Mater.*, 2015, DOI: 10.1002/aenm.201402104.
21. K. Saravanan, C. W. Mason, A. Rudola, K. H. Wong and P. Balaya, *Adv. Energy Mater.*, 2013, **3**, 444-450.
22. C. Zhu, K. Song, P. A. van Aken, J. Maier and Y. Yu, *Nano Lett.*, 2014, **14**, 2175-2180.
23. H. Li, M. Eddaoudi, M. O'Keeffe and O. M. Yaghi, *Nature*, 1999, **402**, 276-279.
24. T. Uemura, N. Yanai and S. Kitagawa, *Chem. Soc. Rev.*, 2009, **38**, 1228-1236.
25. M. Dincă, A. Dailly, Y. Liu, C. M. Brown, D. A. Neumann and J. R. Long, *J. Am. Chem. Soc.*, 2006, **128**, 16876-16883.
26. J. Lee, O. K. Farha, J. Roberts, K. A. Scheidt, S. T. Nguyen and J. T. Hupp, *Chem. Soc. Rev.*, 2009, **38**, 1450-1459.
27. P. Canepa, Y. J. Chabal and T. Thonhauser, *Phys. Rev. B*, 2013, **87**, 094407.
28. M. Kurmoo, *Chem. Soc. Rev.*, 2009, **38**, 1353-1379.
29. K. A. White, D. A. Chengelis, K. A. Gogick, J. Stehman, N. L. Rosi and S. Petoud, *J. Am. Chem. Soc.*, 2009, **131**, 18069-18071.

30. M. D. Allendorf, R. J. T. Houk, L. Andruszkiewicz, A. A. Talin, J. Pikarsky, A. Choudhury, K. A. Gall and P. J. Hesketh, *J. Am. Chem. Soc.*, 2008, **130**, 14404-14405.
31. P. Canepa, K. Tan, Y. Du, H. Lu, Y. J. Chabal and T. Thonhauser, *J. Mater. Chem. A*, 2015, **3**, 986-995.
32. C. H. Hendon, D. Tiana and A. Walsh, *Phys. Chem. Chem. Phys.*, 2012, **14**, 13120-13132.
33. K. T. Butler, C. H. Hendon and A. Walsh, *J. Am. Chem. Soc.*, 2014, **136**, 2703-2706.
34. M. Nagarathinam, K. Saravanan, E. J. H. Phua, M. V. Reddy, B. V. R. Chowdari and J. J. Vittal, *Angew. Chem. Int. Ed.*, 2012, **51**, 5866-5870.
35. A. Shahul Hameed, M. Nagarathinam, M. Schreyer, M. V. Reddy, B. V. R. Chowdari and J. J. Vittal, *J. Mater. Chem. A*, 2013, **1**, 5721-5726.
36. A. S. Hameed, M. V. Reddy, B. V. R. Chowdari and J. J. Vittal, *Electrochim. Acta*, 2014, **128**, 184-191.
37. P. Nie, L. Shen, H. Luo, H. Li, G. Xu and X. Zhang, *Nanoscale*, 2013, **5**, 11087-11093.
38. J. Wang, L. Zhang, L. Yu, Z. Jiao, H. Xie, X. W. Lou and X. Wei Sun, *Nat. Commun.*, 2014, **5**, 4921.
39. C. D. Wessells, R. A. Huggins and Y. Cui, *Nat. Commun.*, 2011, **2**, 550.
40. C. D. Wessells, S. V. Peddada, R. A. Huggins and Y. Cui, *Nano Lett.*, 2011, **11**, 5421-5425.
41. M. Pasta, C. D. Wessells, R. A. Huggins and Y. Cui, *Nat. Commun.*, 2012, **3**, 1149.
42. M. Pasta, C. D. Wessells, N. Liu, J. Nelson, M. T. McDowell, R. A. Huggins, M. F. Toney and Y. Cui, *Nat. Commun.*, 2014, **5**, 3007.
43. Y. Lu, L. Wang, J. Cheng and J. B. Goodenough, *Chem. Commun.*, 2012, **48**, 6544-6546.
44. P. Nie, L. Shen, H. Luo, B. Ding, G. Xu, J. Wang and X. Zhang, *J. Mater. Chem. A*, 2014, **2**, 5852-5857.
45. R. Y. Wang, C. D. Wessells, R. A. Huggins and Y. Cui, *Nano Lett.*, 2013, **13**, 5748-5752.
46. Y. Mizuno, M. Okubo, E. Hosono, T. Kudo, K. Oh-ishi, A. Okazawa, N. Kojima, R. Kurono, S.-i. Nishimura and A. Yamada, *J. Mater. Chem. A*, 2013, **1**, 13055-13059.
47. S. Liu, G. L. Pan, G. R. Li and X. P. Gao, *J. Mater. Chem. A*, 2015, **3**, 959-962.
48. R. Y. Wang, B. Shyam, K. H. Stone, J. N. Weker, M. Pasta, H.-W. Lee, M. F. Toney and Y. Cui, *Adv. Energy Mater.*, 2015, DOI: 10.1002/aenm.201401869.
49. H.-W. Lee, M. Pasta, R. Y. Wang, R. Ruffo and Y. Cui, *Faraday Discuss.*, 2014, **176**, 69-81.
50. P. Canepa, N. Nijem, Y. J. Chabal and T. Thonhauser, *Phys. Rev. Lett.*, 2013, **110**, 026102.
51. X. Wu, W. Deng, J. Qian, Y. Cao, X. Ai and H. Yang, *J. Mater. Chem. A*, 2013, **1**, 10130-10134.
52. F.-S. Ke, Y.-S. Wu and H. Deng, *J. Solid State Chem.*, 2015, **223**, 109-121.
53. A. Kumar, S. M. Yusuf and L. Keller, *Phys. Rev. B*, 2005, **71**, 054414.
54. L. Shen, B. Ding, P. Nie, G. Cao and X. Zhang, *Adv. Energy Mater.*, 2013, **3**, 1484-1489.
55. A. Kumar, S. Yusuf and L. Keller, *Phys. Rev. B*, 2005, **71**, 054414.
56. Z. Wang, H. Wang, B. Liu, W. Qiu, J. Zhang, S. Ran, H. Huang, J. Xu, H. Han, D. Chen and G. Shen, *ACS Nano*, 2011, **5**, 8412-8419.
57. X. Lu, G. Wang, T. Zhai, M. Yu, S. Xie, Y. Ling, C. Liang, Y. Tong and Y. Li, *Nano Lett.*, 2012, **12**, 5376-5381.
58. F. Han, L. Ma, Q. Sun, C. Lei and A. Lu, *Nano Res.*, 2014, **7**, 1706-1717.
59. Y. You, X.-L. Wu, Y.-X. Yin and Y.-G. Guo, *J. Mater. Chem. A*, 2013, **1**, 14061-14065.
60. L. Wang, Y. Lu, J. Liu, M. Xu, J. Cheng, D. Zhang and J. B. Goodenough, *Angew. Chem. Int. Ed.*, 2013, **52**, 1964-1967.
61. X. Wang, B. Liu, Q. Xiang, Q. Wang, X. Hou, D. Chen and G. Shen, *ChemSusChem*, 2014, **7**, 308-313.
62. B. Liu, J. Zhang, X. Wang, G. Chen, D. Chen, C. Zhou and G. Shen, *Nano Lett.*, 2012, **12**, 3005-3011.
63. H. Kim, J. Hong, K.-Y. Park, H. Kim, S.-W. Kim and K. Kang, *Chem. Rev.*, 2014, **114**, 11788-11827.
64. G. Pang, P. Nie, C. Yuan, L. Shen, X. Zhang, J. Zhu and B. Ding, *Energy Technol.*, 2014, **2**, 705-712.
65. Y. Yue, Z. Zhang, A. J. Binder, J. Chen, X. Jin, S. H. Overbury and S. Dai, *ChemSusChem*, 2015, **8**, 177-183.
66. M. Sathiya, G. Rousse, K. Ramesha, C. P. Laisa, H. Vezin, M. T. Sougrati, M. L. Doublet, D. Foix, D. Gonbeau, W. Walker, A. S. Prakash, M. Ben Hassine, L. Dupont and J. M. Tarascon, *Nat. Mater.*, 2013, **12**, 827-835.
67. M. Ati, M. T. Sougrati, G. Rousse, N. Recham, M. L. Doublet, J. C. Jumas and J. M. Tarascon, *Chem. Mater.*, 2012, **24**, 1472-1485.
68. K. Itaya, T. Ataka, S. Toshima and T. Shinohara, *J. Phys. Chem.*, 1982, **86**, 2415-2418.
69. A. A. Karyakin, *Electroanalysis*, 2001, **13**, 813-819.
70. K. Itaya, I. Uchida and V. D. Neff, *Acc. Chem. Res.*, 1986, **19**, 162-168.